Morphometric fingerprints and downslope evolution in bathymetric surveys: insights into morphodynamics of the Congo canyon-channel

Martin Hasenhündl[1,2]*, Peter J. Talling[3,4], Ed L. Pope[4],
Megan L. Baker[4], Maarten S. Heijnen[5], Sean C. Ruffell[3],
Ricardo da Silva Jacinto[6], Arnaud Gaillot[6], Sophie Hage[6],
Stephen M. Simmons[7], Catharina J. Heerema[3,8],
Claire McGhee[9], Michael A. Clare[5] and Matthieu J. B. Cartigny[4]

[1]Institute of Hydraulic Engineering and Water Resources Management, TU Wien, Vienna, Austria,
[2]Institute for Hydraulic Engineering and Hydrometry, Federal Agency for Water Management, Vienna,
Austria, [3]Department of Earth Science, Durham University, Durham, United Kingdom, [4]Department of
Geography, Durham University, Durham, United Kingdom, [5]National Oceanography Centre
Southampton, Southampton, United Kingdom, [6]Geo-Ocean, UMR6538, University Brest, Ifremer,
CNRS, Plouzané, France, [7]Energy and Environment Institute, University of Hull, Hull, United Kingdom,
[8]Expert Analytics, Oslo, Norway, [9]School of Civil Engineering and Geosciences, Newcastle University,
Newcastle upon Tyne, United Kingdom

Submarine canyons and channels are globally important pathways for sediment,
organic carbon, nutrients and pollutants to the deep sea, and they form the
largest sediment accumulations on Earth. However, studying these remote
submarine systems comprehensively remains a challenge. In this study, we
used the only complete-coverage and repeated bathymetric surveys yet for
a very large submarine system, which is the Congo Fan off West Africa.
Our aim is to understand channel-modifying features such as subaqueous
landslides, meander-bend evolution, knickpoints and avulsions by analyzing
their morphometric characteristics. We used a new approach to identify
these channel-modifying features via morphometric fingerprints, which allows
a systematic and efficient search in low-resolution bathymetry data. These
observations have led us to identify three morphodynamic reaches within the
Congo Canyon-Channel. The upper reach of the system is characterized by
landslides that can locally block the channel, storing material for extended
periods and re-excavating material through a new incised channel. The middle
reach of the system is dominated by the sweep and swing of meander
bends, although their importance depends on the channel's age, and the
time since the last up-channel avulsion. In the distal and youngest part
of the system, an upstream migrating knickpoint is present, which causes
multi-stage sediment transport and overspill through an underdeveloped
channel with shallow depths. These findings complement previous less-
detailed morphometric analyses of the Congo Canyon-Channel, offering a
clearer understanding of how submarine canyon-channels can store sediment
(due to channel-damming landslides, meander point bars, levee building
due to overspill), re-excavate that sediment (via thalweg incision, meander
propagation, knickpoint migration) and finally transport it to the deep sea.

This improved understanding of the morphodynamics of the Congo Canyon-Channel may help to understand the evolution of other submarine canyon-channels, and assessment of hazards faced by seabed infrastructure such as telecommunication cables.

1 Introduction

Earth's largest canyon and channel systems are situated on the seafloor (Harris and Whiteway, 2011). Turbidity currents, responsible for shaping these canyons and channels, are notoriously challenging to measure in action, leading to a limited understanding of their dynamics. These flows transport extremely large volumes of sediment, organic carbon, and pollutants from land to the deep sea (Galy et al., 2007; Kane and Clare, 2019; Talling et al., 2022; Pierdomenico et al., 2023), in episodic events lasting from minutes to weeks (Azpiroz-Zabala et al., 2017; Talling et al., 2023). They contribute to the formation of submarine fans, Earth's largest sediment accumulations, while posing a hazard to modern infrastructure, such as ocean-bottom telecommunication lines, which handle more than 99% of global intercontinental data traffic (Carter et al., 2014; Clare et al., 2023).

Some of the most detailed measurements of deep-sea turbidity currents come from the Congo submarine system (Azpiroz-Zabala et al., 2017; Simmons et al., 2020; Talling et al., 2022), which is still directly connected to the Congo River, the world's second-largest river by discharge (Milliman and Farnsworth, 2011). Notably, these observations include the longest sediment flow (of any type) yet monitored in action (Talling et al., 2022), which ran out for over 1,100 km in January 2020. This flow severed both telecommunications cables to West Africa and eroded ~2.65 km^3 of sediment, equivalent to 19%–35% of the global annual riverine sediment flux.

A submarine 'canyon' is defined here as a deeply incised conduit, which may have a series of terraces. In contrast, a submarine 'channel' is less deeply incised, so that turbidity currents may overspill its flanking levees (Qin et al., 2016; Lemay et al., 2020), and the floor of the channel may approach or lie above the elevation of the surrounding seabed. Turbidity currents moving down canyons or channels may cause 'channel or canyon modifying features', such as landslide-dams, meanders, knickpoints and avulsions.

Submarine landslides that can dam canyons or channels have only been detected in rare instances where repeated multibeam bathymetric surveys have been performed (Biscara et al., 2013; Pope et al., 2022b; Talling et al., 2022) or inferred from landslide scars or deposits (Babonneau et al., 2002; Smith et al., 2005; Mountjoy et al., 2009; Ortiz-Karpf et al., 2015).
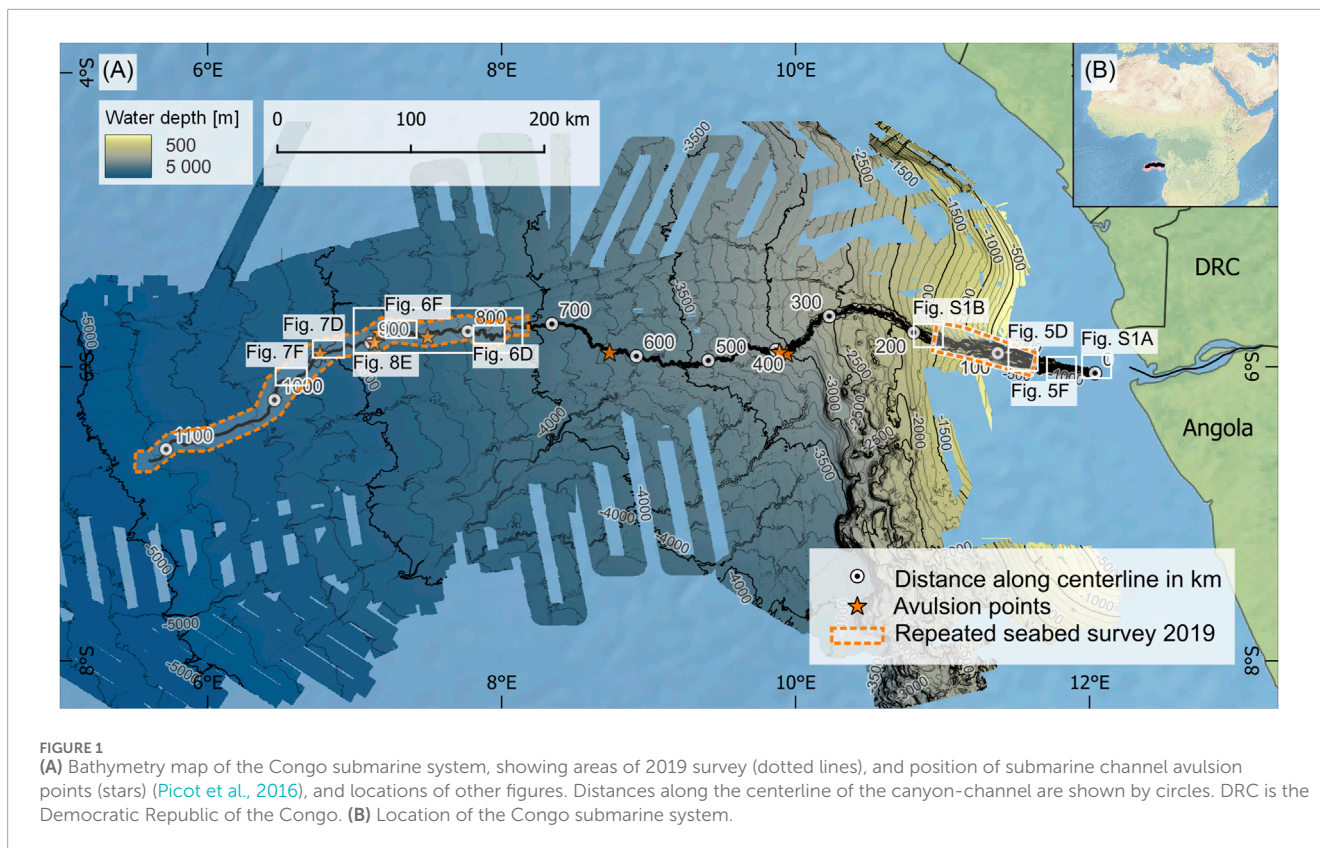
Meander-bend characteristics have been studied extensively in rivers, where bend migration can be composed of downstream-translation (sweep) and lateral-translation (swing), which may result from outer-bend erosion and inner-bend deposition (Leopold and Wolman, 1960; Constantine et al., 2014; Sylvester et al., 2019). Whether similar swing or sweep patterns are also found in submarine systems is the subject of much debate (Palm et al., 2021), with conclusions ranging from absence of pronounced sweep and

swing (Peakall et al., 2000), to bend migration mainly via lateral propagation (Babonneau et al., 2010; Sylvester et al., 2011; Peakall and Sumner, 2015), or via downstream bend translation with lateral translation (Kastens and Shor, 1986; Deptuck et al., 2007; Straub et al., 2008; Morelli et al., 2022).

Steep steps in submarine channels and canyon, known as knickpoints, have been observed in a wide range of shallow submarine systems (<600 m water depth). Their migration patterns and rates have been documented using repeated bathymetry (Guiastrennec-Faugas et al., 2020; Heijnen et al., 2020). However, detailed observations in deeper-water systems are lacking, with knickpoints only identified through peaks in thalweg gradients (Pirmez and Flood, 1995; Pirmez et al., 2000; Babonneau et al., 2002; Heiniö and Davies, 2007; Casalbore et al., 2018; Gales et al., 2019; Tek et al., 2021), or seismic data (Tek et al., 2021). Time lapse surveys were previously lacking in deep-water systems to determine how knickpoints evolve. Avulsions, abrupt changes in channel course, have also been inferred from bathymetry data or seismic data (Amir et al., 1996; Kolla, 2007; Ortiz-Karpf et al., 2015; Picot et al., 2016).

Previous studies have focused on individual channel-modifying features in specific sections of different submarine systems, or on a classification based on geometric characteristics of the entire canyon-channel system (e.g., canyon depth, canyon width, canyon cross-section) (Pirmez and Flood, 1995; Babonneau et al., 2002; Lemay et al., 2020; Bührig et al., 2022). However, as more detailed or time lapse bathymetric data becomes available, there are now opportunities for more detailed and systematic morphological analyses to understand submarine canyon and channel processes (Hasenhündl et al., 2023). Such detailed analyses may also mitigate risk to ocean-bottom infrastructure, such as submarine cables (Talling et al., 2022).

In this study, we use two bathymetric datasets (collected in 1994/1998 and 2019) for one of the largest submarine canyon-channel systems, the Congo Fan offshore West Africa. These datasets are the only time lapse measurements for such a large submarine canyon-channel. We conduct a comprehensive analysis of 12 morphometric characteristics (e.g., thalweg gradient, curvature, sinuosity, meander wavelength, levee slope) for both datasets, based on an active channel approach (Hasenhündl and Blanckaert, 2022). First, we study detailed morphometric characteristics to define novel morphometric fingerprints (distinct changes in morphometric characteristics) of four channel-modifying features, which are (i) damming landslides (and their remnants), (ii) sweep and swing of meander-bends, (iii) knickpoints, and (iv) avulsions. Second, we investigate whether these morphometric fingerprints can identify previously unrecognized features systematically and efficiently. Last, we aim to delineate distinct reaches of the Congo Canyon-Channel based on the morphometric characteristics of the active channel, including channel-modifying features.

FIGURE 1
(A) Bathymetry map of the Congo submarine system, showing areas of 2019 survey (dotted lines), and position of submarine channel avulsion points (stars) (Picot et al., 2016), and locations of other figures. Distances along the centerline of the canyon-channel are shown by circles. DRC is the Democratic Republic of the Congo. **(B)** Location of the Congo submarine system.

2 Background to the site: Congo submarine system

The Congo submarine system extends for 760 km from the coast and continental shelf (Figure 1; Babonneau et al., 2002), and it is one of Earth's largest submarine fans. The upstream part of the system (from the shore to ~200 km offshore) is incised deeply into the continental shelf and slope, forming a submarine canyon that is 6–12 km wide, and >800 m in depth. Around 200 km offshore, the system transitions to a less deeply incised submarine channel that is ~1,200 m wide and 100 m deep. This channel terminates at a water depth of about 5,000 m (~760 km offshore), beyond which there is the area of sediment accumulation termed a lobe. The head of the Congo Canyon lies in the Congo River estuary. Annually, the Congo River delivers ~43 Mt of sediment, and 2 Mt of particulate organic carbon, into the head of the submarine canyon (Coynel et al., 2005). Monitoring studies have demonstrated high activity in the upper canyon, with multiple occurrences of turbidity currents observed each year (Khripounoff et al., 2003; Azpiroz-Zabala et al., 2017; Talling et al., 2022).
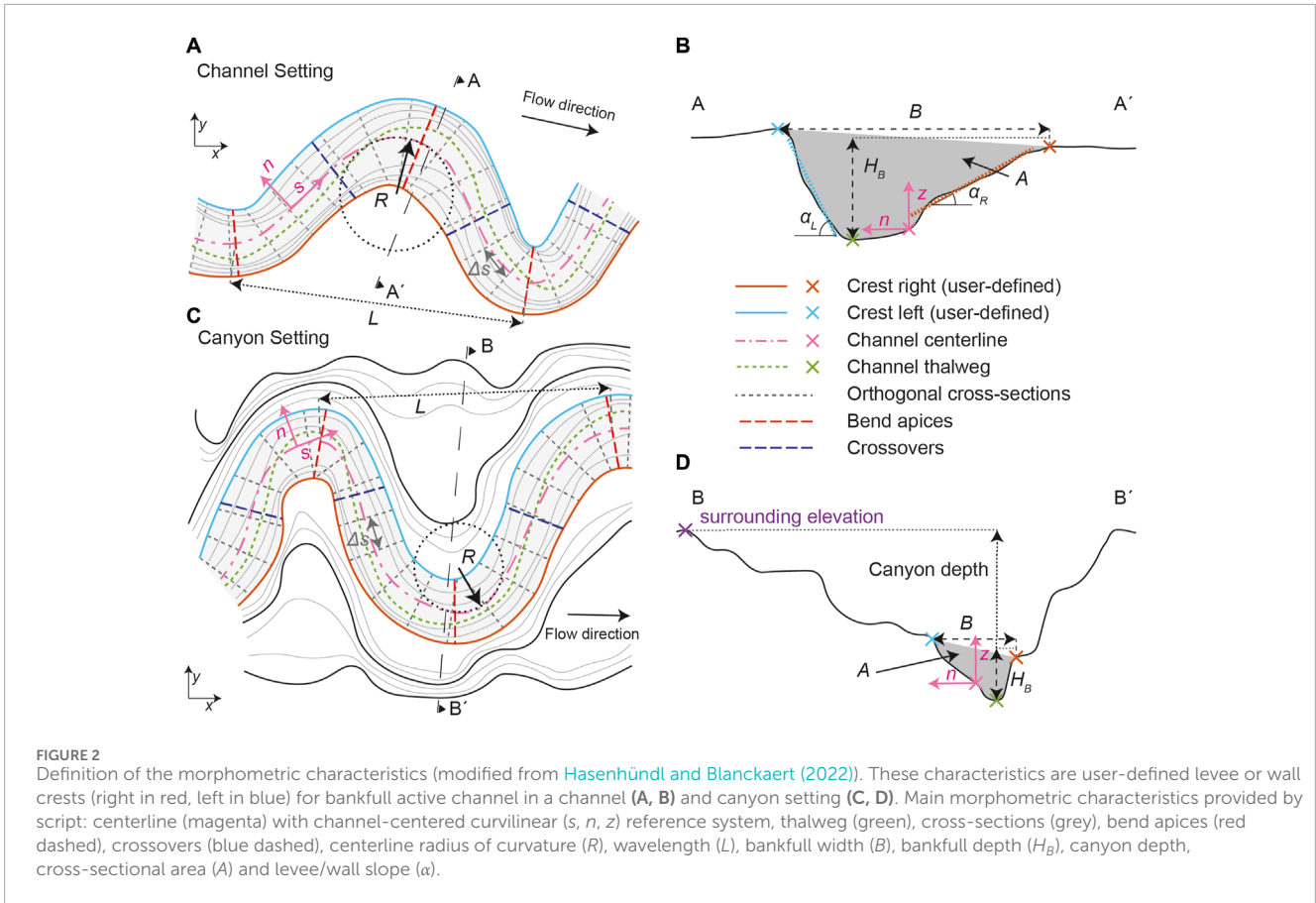
3 Materials and methods

Two bathymetric data sets form the basis of this analysis. The first dataset was collected in 1992–2011 (available via Ifremer Geo-Ocean (2018)), and it covers most of the submarine fan. The deeper-water submarine channel survey data were collected during the GUINESS cruises in 1994 (upstream of

kilometer 650 along the centerline) and ZAIANGO cruises in 1998 (downstream of kilometer 650 along the centerline), in both cases using a Simrad EM12 dual swath multibeam system on board the RV *L'Atalante*. These data were provided in merged data-set with a lower resolution 100 m grid spacing (Babonneau et al., 2002).

The second bathymetric data set was collected during cruise JC187 in 2019 using a Kongsberg EM122 system on board the RRS *James Cook* (Ruffell et al., 2022). This later survey only covered the axial parts of the upper submarine canyon and lowermost submarine channel (Figure 1). For the analysis carried out here, the 2019 data were uniformly resampled to a 15 m grid.

The morphometric characteristics were computed using the methods of analysis described in Hasenhündl and Blanckaert (2022). This approach uses a centerline of the bankfull active channel, which is defined using midpoints of the channel levee crests (Konsoer et al., 2013; Qin et al., 2016; Shumaker et al., 2018). In the submarine canyon, the edges of the first terrace confine the bankfull active channel and are used for the midpoint calculation. (see Figure 2). This method differs from previous methodologies applied to large submarine fans. They either considered the entire canyon for morphometric analysis or used the thalweg as a reference line (Pirmez and Flood, 1995; Babonneau et al., 2002; Shumaker et al., 2018; Palm et al., 2021).

To enable comparison between datasets, the 1994/1998 centerline remained unchanged for the more recent bathymetric data from 2019. A channel-centered curvilinear reference system (s, n, z) was established along the centerline, starting with the

FIGURE 2
Definition of the morphometric characteristics (modified from Hasenhündl and Blanckaert (2022)). These characteristics are user-defined levee or wall crests (right in red, left in blue) for bankfull active channel in a channel **(A, B)** and canyon setting **(C, D)**. Main morphometric characteristics provided by script: centerline (magenta) with channel-centered curvilinear (*s*, *n*, *z*) reference system, thalweg (green), cross-sections (grey), bend apices (red dashed), crossovers (blue dashed), centerline radius of curvature (*R*), wavelength (*L*), bankfull width (*B*), bankfull depth (H_B), canyon depth, cross-sectional area (*A*) and levee/wall slope (*α*).

beginning of the bathymetric data about 70 km from the Congo Estuary (see Figure 1). The resulting *s*-coordinate corresponds to the downstream distance along the active channel centerline, the *n*-coordinate indicates the perpendicular distance to the centerline (*n*-axis positive towards the left crest in flow direction), and the *z*-coordinate represents water depth as illustrated in Figure 2. The *s*-coordinate step size was set at 250 m. At each interval along the centerline, cross-sections were generated to determine several characteristics including bankfull width (*B*), bankfull channel depth (H_B), cross-sectional area (*A*), channel aspect ratio (B/H_B), top elevation of right (z_R) and left crest (z_L), slope of right ($α_R$) and slope of left levee/wall ($α_L$; transverse slope of levee/terrace wall, excluding the flat channel bottom) and thalweg position (n_T) (Figure 2). These characteristics were smoothed over a 1 km window (moving median) to account for outliers.

The Matlab script also computed longitudinal characteristics such as radius of curvature (*R*), bend apices (where by definition 1/*R* attains its maximum magnitude), crossovers (channel inflection points where by definition 1/*R*=0), sinuosity (*SI*, the ratio between the distance along centerline and the straight distance between two points) in different step-lengths (from crossover to crossover, fixed step-lengths 10 km, 24.5 km (20 times median *B*) and 250 km) and wavelengths (*L*) along the centerline (see Figure 2). The thalweg (automatically detected by the minimum bed elevation in the cross-section) was used to calculate the longitudinal bottom profile to derive the thalweg gradient (*S*), presented with data smoothed over 10 km and 100 km (moving mean).

The locations and ages of channel avulsions were obtained from Picot et al. (2016), Picot et al. (2019), which were determined using a combination of bathymetric and seismic data at 387 km (~70 kyr), 396 km (~38 kyr), 629 km (~11 kyr), 744 km, 839 km, 887 km, 897 km (~6 kyr) and 943 km (~4 kyr).

4 Results

4.1 General morphology of the Congo Canyon-Channel

The canyon-channel has a centerline that is 1,118 km long, commencing approximately 70 km from the canyon head in the Congo Estuary. The channel reaches a water depth of 5,000 m (Figure 3A). The system's overall thalweg gradient *(S)* averages around 3.5 m/km (0.20°), and this gradient decreases from ~8 m/km (0.46°) at the canyon head, to ~2 m/km (0.11°) around the middle of the system (at ~400 km), and remains relatively constant until the channel's termination (Figure 3B).

In contrast to previous assessments of the entire Congo Canyon-Channel (Babonneau et al., 2002), where the canyon/channel depth decreased uniformly, the bankfull channel depth (H_B) of the active channel shows an initial increase followed by a nearly-constant channel depth (~100 m) across most of the system. Only towards the channel's termination (from ~840 km on, Figure 3C), is there a decrease in channel depth, coinciding with a similar
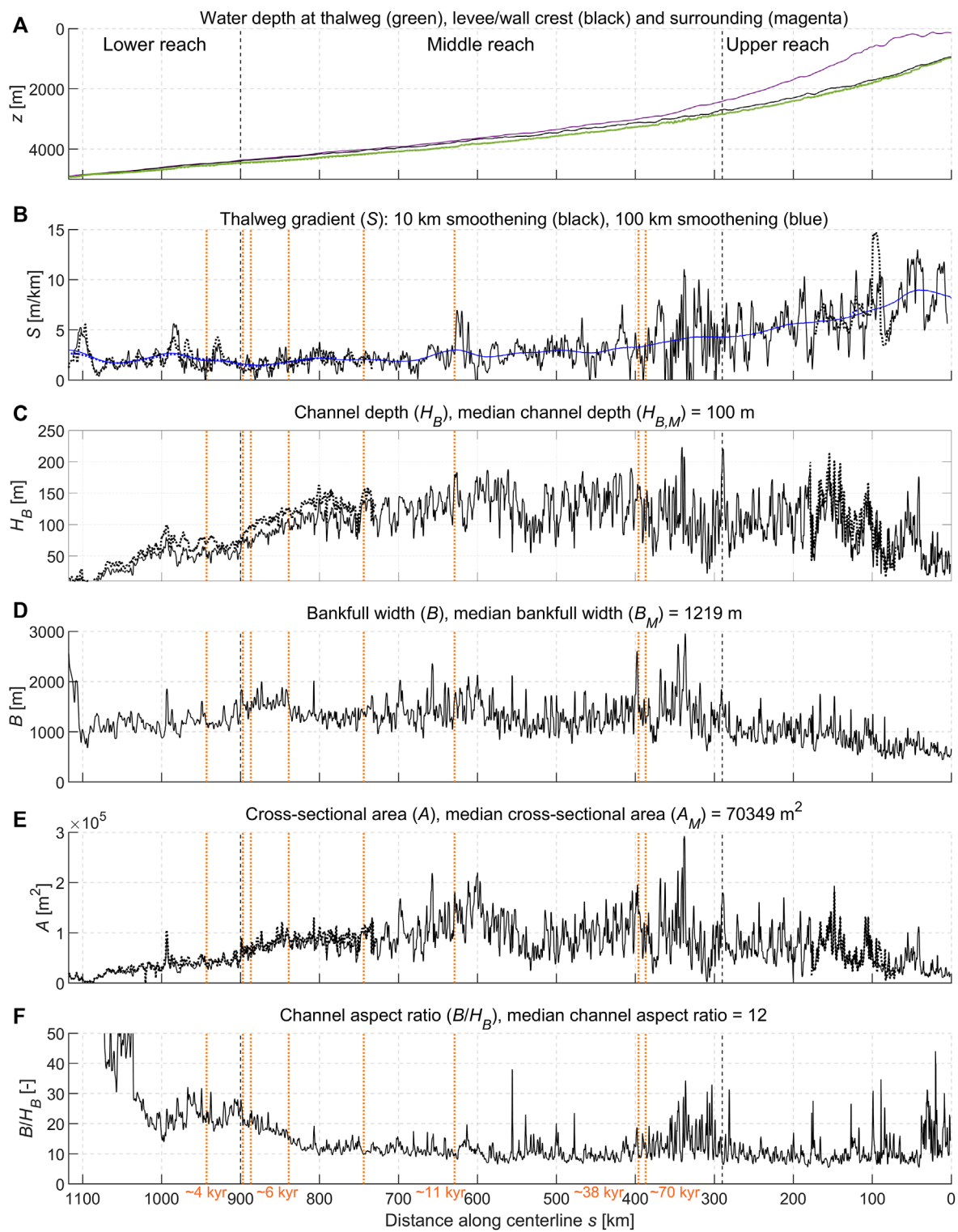
FIGURE 3
Morphometric characteristics of Congo Canyon-Channel: **(A)** longitudinal profile, **(B)** thalweg gradient (S), **(C)** channel depth (H_B), **(D)** bankfull width (B), **(E)** cross-sectional area (A) and **(F)** channel aspect ratio (B/H_B). Characteristics in solid lines are derived from the 1994/1998 data, characteristics in dashed lines are derived from the 2019 data. Vertical black dashed lines separate different morphodynamic reaches in the system. Vertical orange dotted lines indicate avulsions, according to Picot et al. (2016).
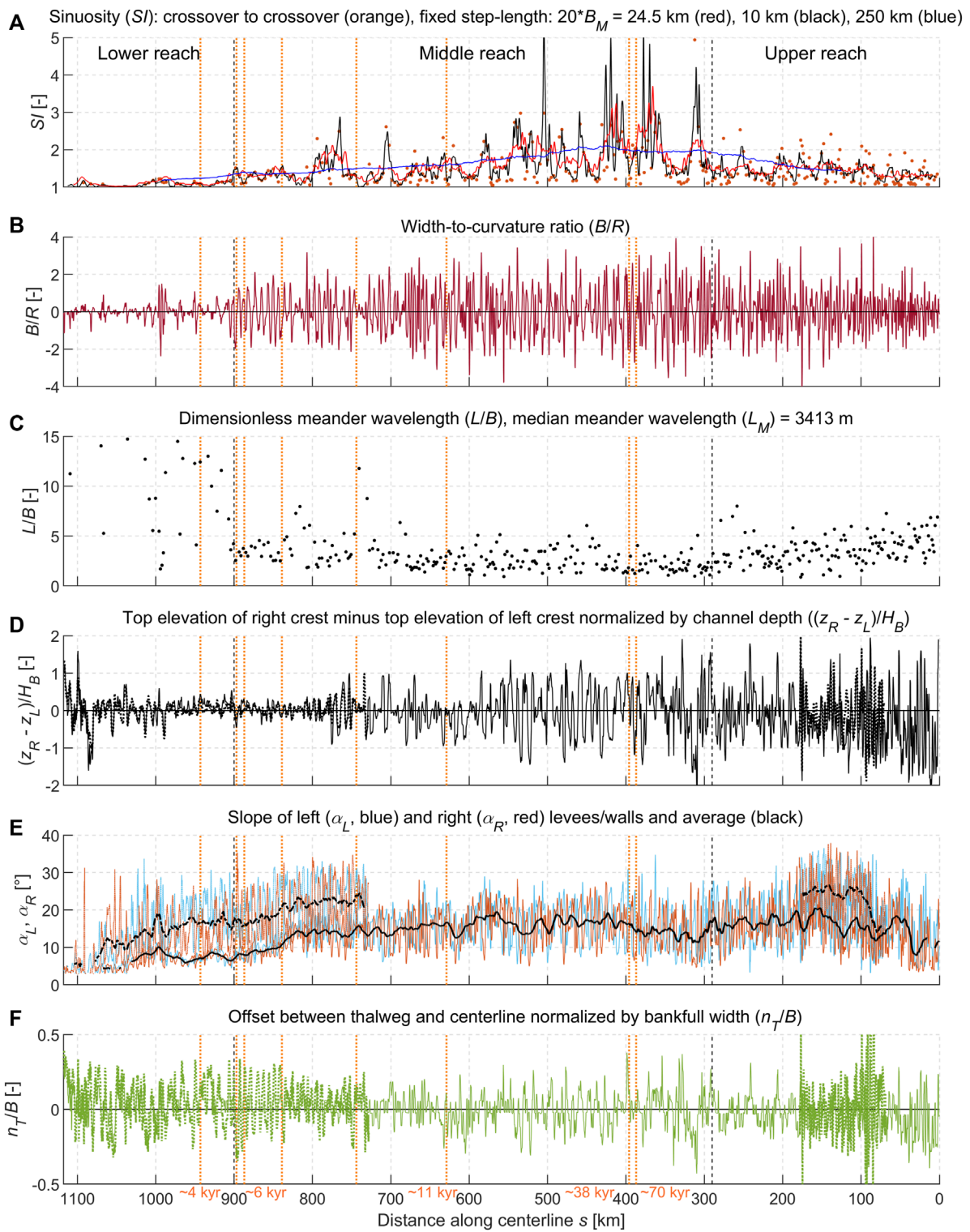
FIGURE 4
Morphometric characteristics of Congo Canyon-Channel: **(A)** sinuosity (SI), **(B)** width-to-curvature ratio (B/R), **(C)** dimensionless meander wavelength (L/B), **(D)** top elevation of right levee/wall crest and left levee/wall crest normalized by channel depth ((z_R - z_L)/H_B), **(E)** levee/wall slopes (α_L, α_R, and average) and **(F)** offset between thalweg and centerline normalized by bankfull width (n_T/B). Characteristics in solid lines are derived from the 1994/1998 data, characteristics in dashed lines are derived from the 2019 data. Vertical black dashed lines separate different morphodynamic reaches in the system. Vertical orange dotted lines indicate avulsions, according to Picot et al. (2016).
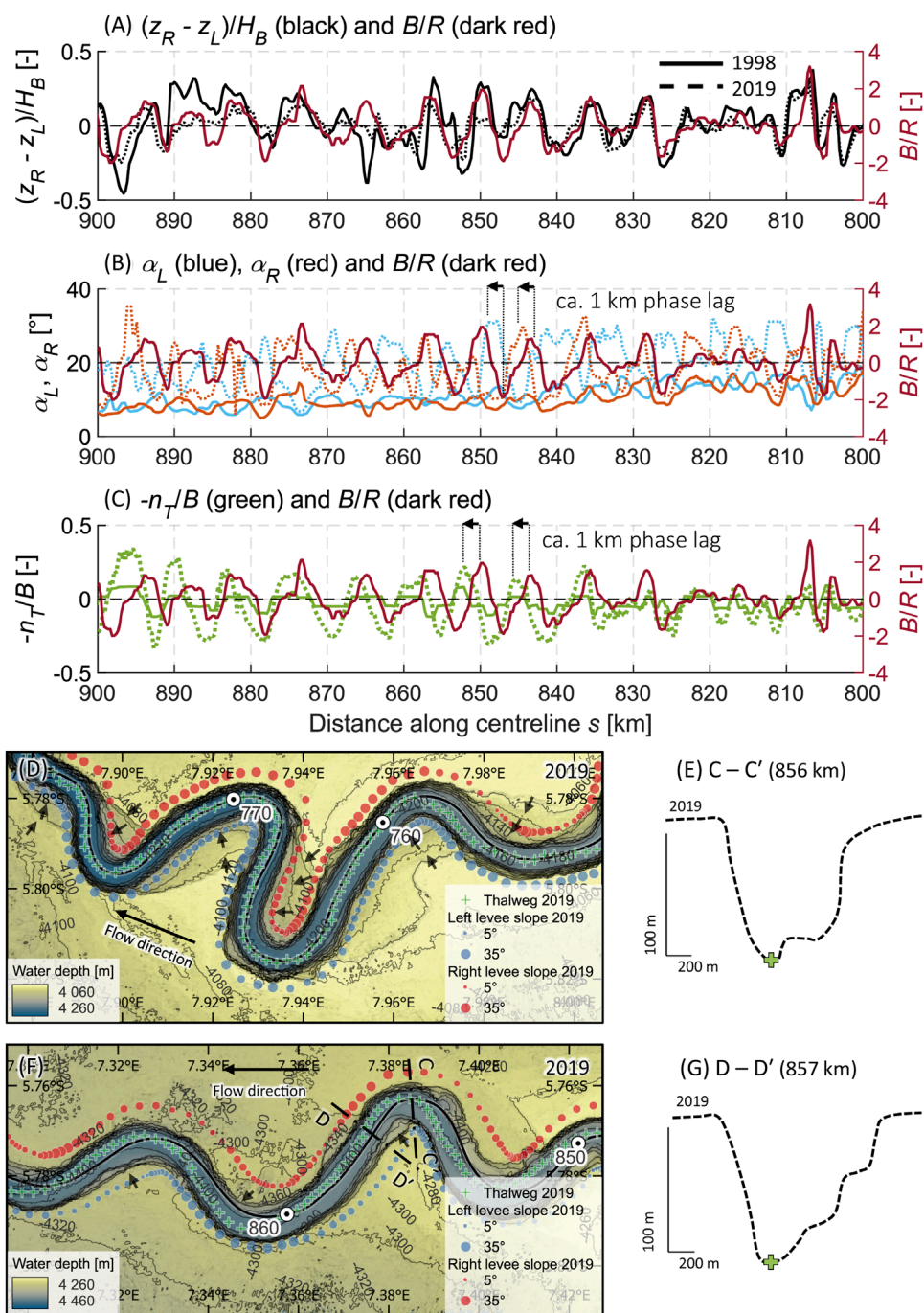
FIGURE 5
Morphometric fingerprint of channel-damming landslides. **(A)** Detailed section of channel's longitudinal profile, showing the ca. 100 m infill occurred in the 2019 data (dashed line, white arrow, 95 km) and similar sized infill in the original 1994 data (solid line, striped arrow, 40 km). **(B)** Peaks in thalweg gradient at landslide locations with possible older landslides in the original 1994 data identified from thalweg gradient and levee slope (dotted arrows, detailed in Supplementary Figure S1). **(C)** Decreasing terrace wall slope at landslide locations (2019—dashed line, 1994—solid line). **(D, E)** Channel-damming landslide at 95 km in 2019 data (white arrow) and **(F, G)** at 40 km in 1994 data (striped arrow).

decline in cross-sectional area (A) (Figure 3E). The bankfull width (B) maintains consistency at about 1,200 m throughout the entire system (Figure 3D). Consequently, the median aspect ratio (B/H_B) remains around 12 for most of the system (Figure 3F), aligning with typical values observed in submarine systems (Konsoer et al., 2013; Shumaker et al., 2018; Lemay et al., 2020; Hasenhündl et al., 2023).

Sinuosity (SI) ranges between 1.5 and 2 over large spatial steps (step-length of 250 km), and shows peak values reaching up to 5 at small spatial steps (step-lengths from crossover to
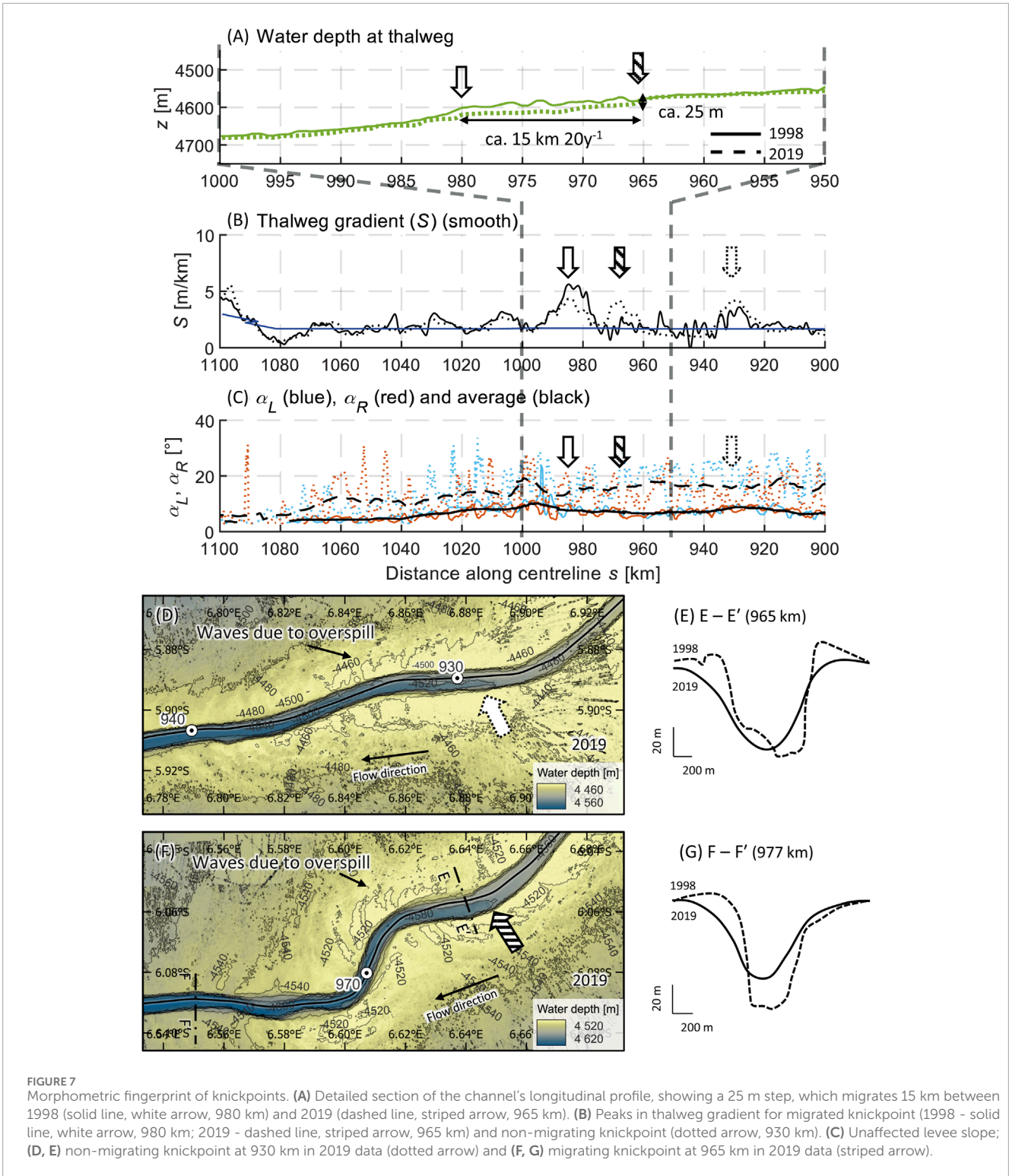
FIGURE 6
Morphometric fingerprint of sweep and swing meanders. **(A)** Difference of levee crest elevations ($(z_R−z_L)/H_B$) correlating with width-to-curvature ratio (B/R). **(B)** Levee slope (α_L, α_R) with 1 km phase lag to width-to-curvature ratio (B/R) and **(C)** thalweg offset (for better visualization axis sign swapped for n_T/B) with 1 km phase lag to width-to-curvature-ratio (B/R). Characteristics in solid lines are derived from the 1998 data, characteristics in dashed lines are derived from the 2019 data. **(D,E,F, G)** Bathymetry of 2019 survey with visualized thalweg (green stars), levee slopes (size of blue and red dots), direction of meander migration and resulting terraces (small black arrows) and point bars.

crossover, 10 km and 24.5 km, Figure 4A). The width-to-curvature ratio (B/R) reveals regular maxima of 2 (Figure 4B), while the dimensionless meander wavelength (L/B) mostly remains below 5 (Figure 4C), consistent with typical values in submarine channels (Lemay et al., 2020; Hasenhündl et al., 2023), with

irregular values at the end of the system due to the almost rectilinear course.

An asymmetrical behavior in levee/wall crest elevation along the active channel is evident through the disparity in right and left levee/wall crest elevations normalized by the channel depth
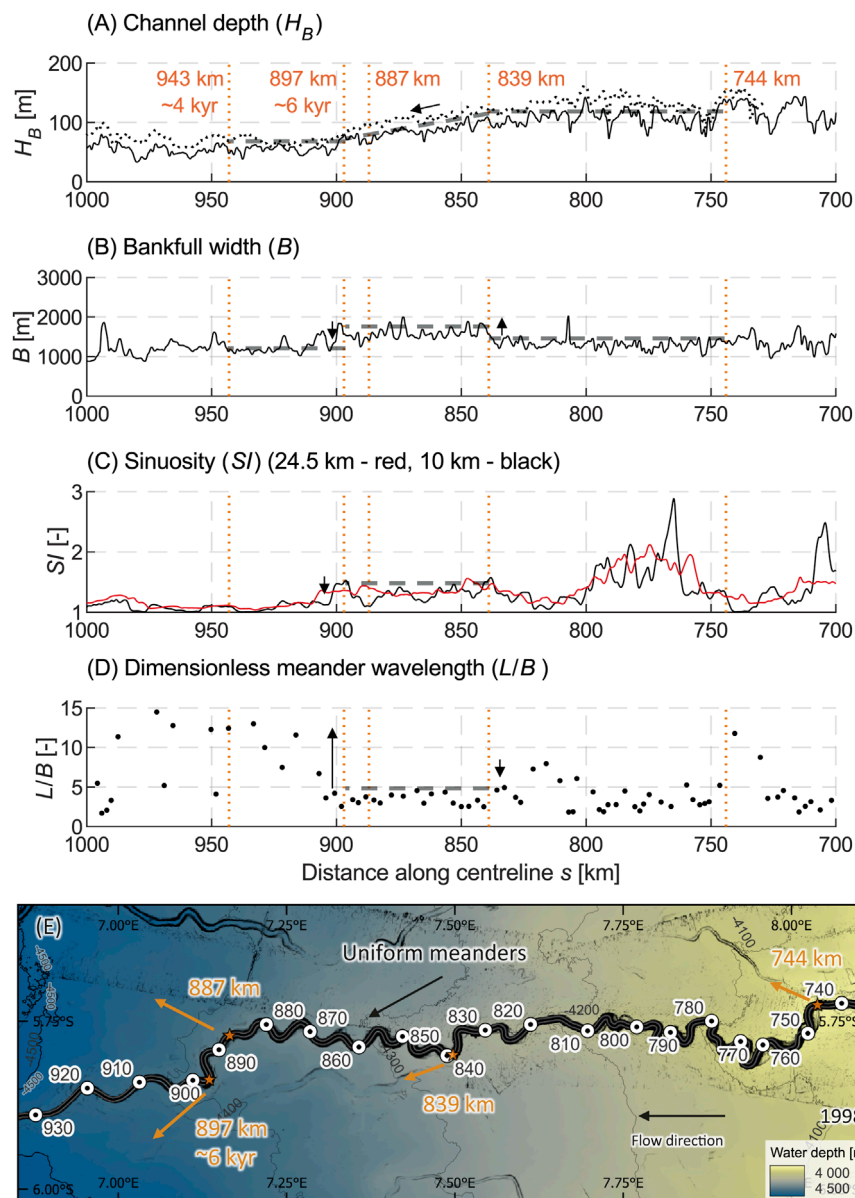
FIGURE 7
Morphometric fingerprint of knickpoints. **(A)** Detailed section of the channel's longitudinal profile, showing a 25 m step, which migrates 15 km between 1998 (solid line, white arrow, 980 km) and 2019 (dashed line, striped arrow, 965 km). **(B)** Peaks in thalweg gradient for migrated knickpoint (1998 - solid line, white arrow, 980 km; 2019 - dashed line, striped arrow, 965 km) and non-migrating knickpoint (dotted arrow, 930 km). **(C)** Unaffected levee slope; **(D, E)** non-migrating knickpoint at 930 km in 2019 data (dotted arrow) and **(F, G)** migrating knickpoint at 965 km in 2019 data (striped arrow).

$((z_R - z_L)/H_B$; Figure 4D), diverging from earlier descriptions of symmetrical levees (Babonneau et al., 2002; Baudin et al., 2017). The average levee/wall slope in the 1994/98 dataset ranges at around ~16° across large portions of the system and around 24° in the higher-resolution 2019 dataset. This discrepancy is expected due to enhanced levee/wall mapping precision with increased resolution. However, in both datasets, the trend in levee slope consistently declines from around ~840 km towards the end of the channel (Figure 4E). The channel's asymmetry is described by the absolute offset between the thalweg and the centerline (n_T), normalized by bankfull width (B). Throughout the system, this thalweg offset to the centerline (n_T) reaches up to about 30% of the bankfull width (B) (Figure 4F).

FIGURE 8
Examples of morphometric fingerprints of avulsions. **(A)** Bankfull channel depth, showing a decrease between 839 km and 897 km. **(B)** Bankfull width, showing an increase between 839 km and 897 km. **(C)** Homogeneous sinuosity between 839 km and 897 km followed by a drop. **(D)** Homogeneous dimensionless meander wavelength between 839 km and 897 km followed by irregular values downstream. **(E)** Position of avulsions (stars) (Picot et al., 2016) in the 1998 data.

4.2 Channel-modifying features

4.2.1 Channel-damming landslides

A comparative analysis of the 1994 and 2019 bathymetric data reveals a significant morphometric change occurring 95 km downstream of the mapped Congo Canyon-Channel (Figures 5D,E). A canyon flank landslide has dammed the canyon-axis, causing a meander bend cutoff (Pope et al., 2022b). Subsequently, a sediment wedge, approximately ~0.4 ± 0.1 km³ in volume and up to 100 m thick, was deposited behind the landslide, extending for >26 km up-canyon (Pope et al., 2022b).

This channel-damming landslide exhibits a distinct morphometric fingerprint characterized by four key features: (1) an elevation increase in the thalweg due to the infill (Figure 5A), (2) a decline in thalweg gradient (S) upstream of the landslide dam caused by the infill behind this blockage, (3) followed by a short but substantial peak in S on the downstream side of the landslide dam (Figure 5B), and (4) a decrease in terrace wall slopes (α_R, α_L and average) upstream of the landslide attributed to the buried original walls due to infilling (Figure 5C).

A previously unidentified channel-damming landslide, of comparable size and preservation, is identified at 40 km in the older

1994 bathymetric data using this distinct morphometric fingerprint. This landslide-dam was infilled by ~80 m of sediment reaching a distance of ~20 km upstream (Figures 5A,F,G). Potentially less well-preserved landslide dams are also identified at 10 km and 190 km. These additional landslide dams might not be easily visible in the bathymetric data without applying these new methods, as detailed in the Supplementary Material.

However, some locations exhibit anomalies that might be mistaken for landslide dams. For example, the step in the thalweg elevation at 50 km (Figure 5A) lacks corresponding reductions in S (Figure 5B) or wall slopes (Figure 5C). Additionally, no identifiable landslide feature is apparent in the bathymetry, suggesting that this step in the profile might be an artefact stemming from the 100 m resolution or the quality of the 1994 data.

4.2.2 Sweep and swing of meander-bends

River meanders are characterized by downstream bend translation (sweep) and lateral translation (swing) of meander bends with high curvatures caused by outer-bend erosion and inner-bend deposition (Leopold and Wolman, 1960; Sylvester et al., 2019). This behavior is observable visually in the 2019 higher resolution data through terrace levels (Figures 6D,F) (Babonneau et al., 2010), with consecutive levels of terraces providing a history of bend migration. Moreover, the sweep and swing meander behavior might be reflected in three distinct morphometric characteristics:

(1) A pronounced asymmetric behavior of levee crests (z_R - z_L, levee crest superelevation) normalized by channel depth (H_B) correlates with the width-to-curvature ratio (B/R) (Figure 6A). This indicates that outer levees tend to be higher than inner levees within a bend (for $B/R > 0$ a left bend, thus outer right levee (z_R) higher than inner left levee (z_L) and therefore (z_R - z_L)/H_B > 0; vice versa for B/R < 0 a right curve, thus (z_R - z_L)/H_B < 0). This is due to a run-up of flow on the outer levees, possibly from a erosive dense bottom layer (Straub et al., 2008; Talling et al., 2022). At the apices (maximum curvature), the levee crest superelevation reaches approximately 30% of H_B (Figure 6A; Figure 9D; Supplementary Table S1).

(2) The bend curvature (B/R) correlates with levee slopes (α_R, α_L), indicating that outer levees are steeper than the inner levees within a bend. The steepest slope of the outer levees is observed 1 km downstream of the apices (Figure 6B; Figures 9I,J; Supplementary Table S1), which may indicate maximum outer levee erosion 1 km downstream of the bend apices, associated with a downstream and outward bend movement (Peakall and Sumner, 2015; Palm et al., 2021).

(3) The thalweg offset (n_T/B) shows a correlation with bend curvature (B/R), with a 1 km downstream phase lag from the apices (Figure 6C; Figure 9O, P; Supplementary Table S1). The thalweg shifts approximately 20% of B towards the outer levee of the bend 1 km downstream of the apex (for $B/R > 0$ a left bend, the thalweg moves to the right outer levee, according to the (s, n, z) reference system an $n < 0$ and vice versa), causing the bend to move downstream and outward (Peakall and Sumner, 2015; Palm et al., 2021). The correlation is more pronounced in the 2019 data due to the higher bathymetry resolution (Figure 9I, O Supplementary Table S1).

These correlations collectively point to both downstream (sweep) and outward (swing) movements of the meander bends (Peakall et al., 2000; Straub et al., 2008; Sylvester et al., 2011; Hansen et al., 2015; Palm et al., 2021), similar to behaviors observed in high-curvature river systems (Sylvester et al., 2019). The downstream phase lag in thalweg offset suggests a downstream deepening, alongside steeper outer levees downstream and levee crests superelevation. This movement leads to progressive downstream and outward shifting of meanders through erosion at the outer bank (bank pull, Figures 6D,F) resulting in asymmetrical cross-section with point bars (Figures 6E,G) (Palm et al., 2021). The progressive swing movement is also reflected in the increased sinuosity (SI) upslope in the middle reach until 290 km (Figure 4A), representing older parts of the system, while the dimensionless meander wavelength (L/B) remains constant (Figure 4C).

4.2.3 Knickpoints

Migrating knickpoints, which are steep steps in channels that migrate upstream via erosion, have been observed in relatively shallow systems (<600 m water depth) (Guiastrennec-Faugas et al., 2020; Heijnen et al., 2020) and have only been identified by peaks in thalweg gradients or longitudinal profiles (Pirmez and Flood, 1995; Pirmez et al., 2000; Babonneau et al., 2002; Heiniö and Davies, 2007; Casalbore et al., 2018; Gales et al., 2019; Tek et al., 2021). A comparison between the 1998 and 2019 bathymetric data of the Congo Channel reveals the migration of a previously identified knickpoint. Initially situated at 980 km in a water depth of ~4,600 m (Babonneau et al., 2002), this ~25 m high knickpoints moved upstream to 965 km over 21 years, migrating approximately 15 km (~750 m/yr).

This migration produces a distinct morphometric fingerprint characterized by three features: (1) a lowered thalweg elevation along the lateral migration in the channel (Figure 7A), (2) a peak in the thalweg gradient (S) represents the knickpoint itself, moving upstream with the migrating knickpoint. No significant drop in S is observed upstream of the steep step, suggesting a lack of infill and an associated landslide (Figure 7B). (3) This is also the reason why there is no visible change in the levee slopes (Figure 7C). Knickpoints lead to thalweg deepening without altering the broader cross-section morphology (Figures 7E,G) (Guiastrennec-Faugas et al., 2020; Heijnen et al., 2020).

Another recognizable knickpoints is found at 930 km, but it does not show clear signs of migration. At 780 km and upstream, no knickpoints were identified in the detailed 2019 data. Babonneau et al. (2002) report a knickpoint at 780 km, which is not observed here. Thus, the purported knickpoint at 780 km reported by Babonneau et al. (2002) might potentially be an artefact, perhaps attributed to the longer (25 km) smoothing distance applied in that study. At 610 km, a significant gradient increase (Figure 3C) along the thalweg could indicate a knickpoint, as noted by Babonneau et al. (2002).

4.2.4 Avulsions

Avulsions are abrupt changes in an active channel's path, and they have traditionally been identified via a combination of bathymetry and seismic data (Amir et al., 1996; Kolla, 2007; Ortiz-Karpf et al., 2015; Picot et al., 2016). However, seismic data

is often not as widely available as bathymetric data (Bührig et al., 2022). To establish potential morphometric fingerprints of avulsions, exclusively using bathymetric data, we analyze morphometric characteristics between different avulsion points (e.g., bankfull channel depth, sinuosity, width-to-curvature and dimensionless meander wavelength). Any consistent changes will be regarded as the morphometric fingerprint of the avulsion.

For example, the channel between avulsion points at 744 km and 839 km maintains a constant bankfull channel depth (H_B) (Figure 3C; Figure 8A), a constant bankfull channel width (B) (Figure 3D; Figure 8B) and an unchanging average levee slope (Figure 4E). Conversely, the following downstream section between avulsion points at 839 km and 897 km shows a notably decreasing H_B (Figure 3C; Figure 8A), an increased but constant B (Figure 3D; Figure 8B), an uniform consistent sinuosity (SI) (Figure 4A; Figure 8C), width-to-curvature ratio (B/R) (Figure 4B), dimensionless meander wavelength (L/B) (Figure 4C; Figure 8D) and a consistently decreasing average levee slope (α_R, α_L) (Figure 4E). At the avulsion point at 897 km, an abrupt change is observed in nearly all morphometric characteristics: a distinct step in H_B (Figure 3C; Figure 8A), B (Figure 3D; Figure 8B), cross-sectional area (A) (Figure 3E) and aspect ratio (B/H_B) (Figure 3F). Additionally, there is an abrupt absence of SI (Figure 4A; Figure 8C) and B/R (Figure 4B) and irregular L/B (Figure 4C; Figure 8D).

4.3 System reaches with distinctive morphodynamics

Three distinct reaches can be delineated based on variations in sinuosity (SI) and slight variations in other characteristics, such as width-to-curvature ratio (B/R) and dimensionless meander wavelength (L/B). These reaches are the upper reach (0–290 km), the middle reach (290–900 km) and the lower reach (900–1,118 km). In the upper reach, SI averages around 1.5 (Figure 4A), B/R consistently peaks below 2 (Figure 4B) and L/B varies between 2 and 6 (Figure 4C). In the middle reach, there are occasional SI peaks reaching 5, but mostly averaging around 2 (Figure 4A), accompanied by B/R consistently maxes out at 2 (Figure 4B) and L/B remains mostly below 5 (Figure 4C). In the lower reach, both SI and B/R significantly drop (Figures 4A,B) and L/B becomes clearly irregular (Figure 4C).

The correlation between levee/wall crest superelevation ((z_R - z_L)/H_B) and width-to-curvature ratio (B/R), previously described for sweep and swing meanders, exhibits a stronger pattern at the bend apices in the upper reach (β_1=0.27–0.33, R^2=0.39–0.43, Supplementary Table S1), followed by those in the middle reach (β_1=0.11–0.19, R^2=0.40–0.53, Supplementary Table S1). In the lower reach, where there are fewer sharp bends (B/R is significantly smaller than in the middle and upper reaches), there is less clarity due to scatter at low B/R, lacking a distinct trend in superelevation (Figures 9A–F, R^2=0.00–0.10; Supplementary Table S1).

With regard to the correlation between B/R and levee/wall slopes (α_R, α_L), there are variations in the positioning of the maximum values within bends across different reaches. The highest wall slope

asymmetry is displayed directly at the apices in the upper reach (Figure 9L, |β_1|=2.16–3.49, R^2=0.22–0.58; Supplementary Table S1). In contrast, the greatest asymmetry and outer levee slope occur 1 km downstream of the apices in the middle reach (Figure 9I), particularly in the higher resolution 2019 data (|β_1|=3.94–4.18, R^2=0.67–0.68, Supplementary Table S1). The results indicate that there is no significant difference between the values obtained directly at the apices and those obtained 1 km downstream in the lower reach. However it should be noted that the values for α_R and α_L are generally lower in the latter case (Figures 9G,H; Supplementary Table S1).
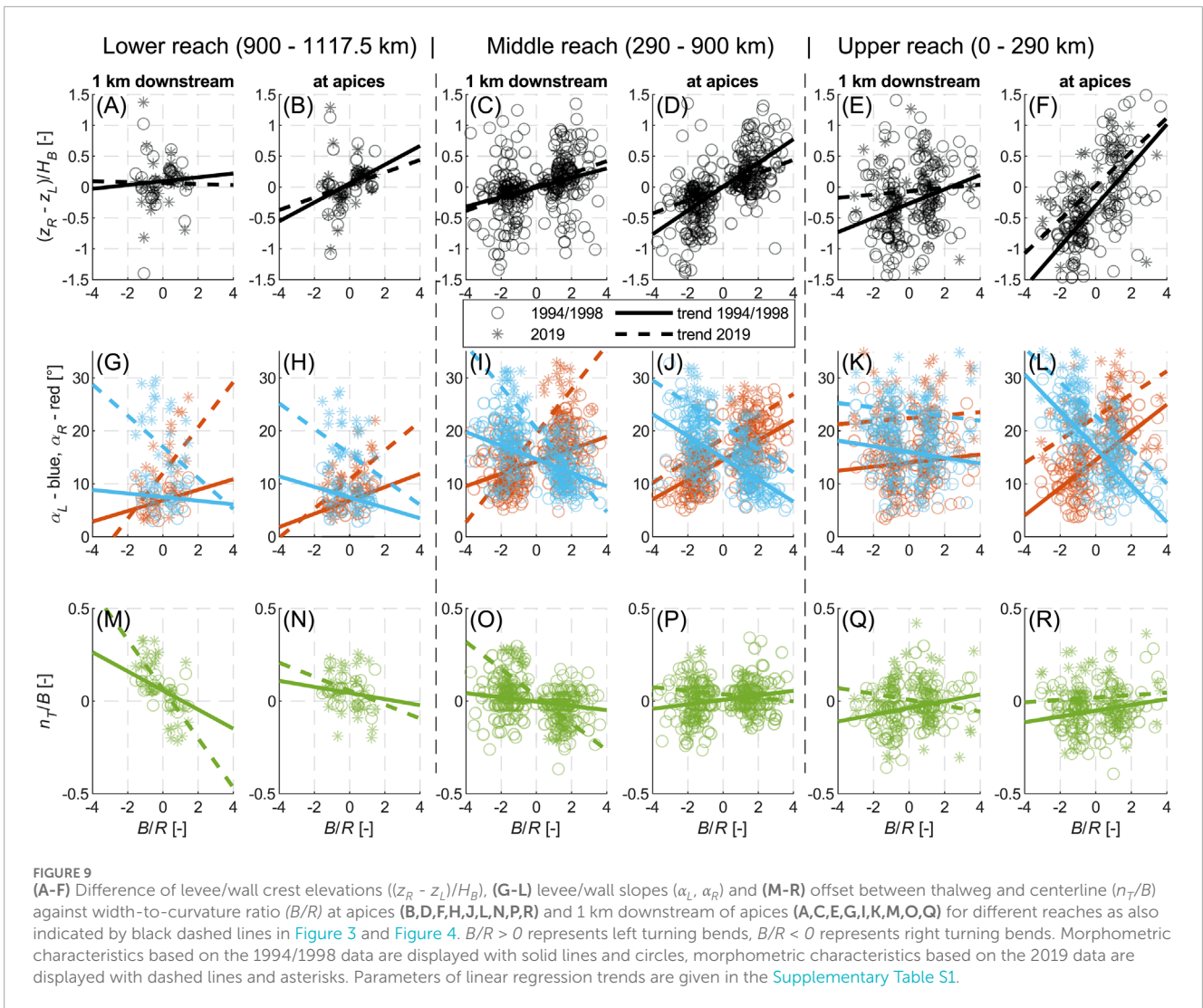
The thalweg offset to the centerline (n_T) in the upper system reach does not show a pronounced trend (Figure 9Q, R, |β_1|=0.01–0.02, R^2=0.01–0.07; Supplementary Table S1). However, in the middle reach, particularly in the higher resolution 2019 data, the thalweg clearly moves 1 km downstream from the apices towards the outside of the bend (Figure 9O, β_1=−0.07, R^2=0.56; Supplementary Table S1). Despite the lower number of sharp bends in the lower reach, there is an observable correlation between curvature and thalweg offset 1 km downstream from the apices (Figure 9M, N, β_1=−0.05–0.13, R^2=0.35–0.47; Supplementary Table S1).

5 Discussion

5.1 Morphometric fingerprints

The identification of landslide-dams involves distinctive features such as increased thalweg elevation, a drop in thalweg gradient (S) followed by a peak downstream in S and decreasing levee/wall slopes (α_R, α_L) upstream of the landslide. This identification of a set of morphometric fingerprints for landslide-dams through two independent characteristics (S and α_R-α_L) allows for a systematic search for these features and can help assess their recurrence rate of these events. The newly identified landslide-dam at 40 km shows preservation qualities comparable to the more recent landslide at 95 km (Pope et al., 2022b), indicating a potential occurrence timeframe preceding the 1994 survey (approximately 5–20 years prior). The presence of additional potential older landslide-dams at 10 km and 190 km suggests that these events might be more frequent than previously assumed (Babonneau et al., 2004).

Typically, the appearance of meandering submarine channels has been described using sinuosity and individual cross-sectional shapes, drawing analogies with fluvial systems (Pirmez and Flood, 1995; Babonneau et al., 2010; Prerna and Mahender, 2020). The addition of information regarding the phase lag in thalweg position and levee slope offers insights into the sweep and swing dynamics of these meanders (Peakall et al., 2000; Straub et al., 2008; Sylvester et al., 2011; 2019). It was presumed that if the maximum thalweg movement and the steepest levee slope occurred at the B/R apex, then the maximum erosion would occur there, and the primary movement would be directed laterally outwards at the apex (Babonneau et al., 2010). Contrary to this assumption, the presence of a 1 km phase lag indicates that the point of maximal erosion of the levees and the thalweg is slightly downstream of the bend. This leads to an additional downstream component of

FIGURE 9
(A-F) Difference of levee/wall crest elevations ((z_R - z_L)/H_B), **(G-L)** levee/wall slopes (α_L, α_R) and **(M-R)** offset between thalweg and centerline (n_T/B) against width-to-curvature ratio (B/R) at apices **(B,D,F,H,J,L,N,P,R)** and 1 km downstream of apices **(A,C,E,G,I,K,M,O,Q)** for different reaches as also indicated by black dashed lines in Figure 3 and Figure 4. B/R > 0 represents left turning bends, B/R < 0 represents right turning bends. Morphometric characteristics based on the 1994/1998 data are displayed with solid lines and circles, morphometric characteristics based on the 2019 data are displayed with dashed lines and asterisks. Parameters of linear regression trends are given in the Supplementary Table S1.

its movement, contributing to a sweep and swing behavior akin to rivers with high curvature (Sylvester et al., 2019). While this behavior may not be directly observable in the repeated bathymetry due to the 100 m resolution of the 1998 data, it becomes apparent when examining the terraces (Figures 6D,F) and comparing the area upstream of the repeated survey (290–725 km, Figure 3). Despite the consistency in morphometric characteristics, the sinuosity increases in the older channel upslope. Essentially, as the channel becomes older, lateral spreading of the meanders intensifies until they encounter limitations imposed by the canyon further upstream.

Knickpoints, identifiable by thalweg gradient peaks (Pirmez and Flood, 1995; Babonneau et al., 2002; Heiniö and Davies, 2007; Heijnen et al., 2020; Guiastrennec-Faugas et al., 2021), can now be differentiated from steep drops caused by damming landslides due to unaffected levee/wall slopes near autogenic knickpoints. The suggested correlation between knickpoints and avulsions by Babonneau et al. (2002) lacks confirmation, with the most noticeable knickpoint located downstream of the youngest avulsion,

which exhibits a migration rate of 15 km per 20 years (~750 m/yr), contrasting with the timescales of avulsions (thousands of years) (Picot et al., 2019).

Sudden changes in morphometric characteristics (e.g., bankfull channel depth, sinuosity, width-to-curvature ratio, meander wavelength, levee slope), which are quite homogeneous over some sections, serve as robust indicators of avulsion, aligning well with previously documented avulsions (Picot et al., 2019). It appears that only the more recent avulsions (situated downstream of 744 km and therefore younger than ~6 kyr (Picot et al., 2019)) are distinguishable in the morphometric characteristics and older avulsions (located upstream of 744 km and thus older than ~11 kyr (Picot et al., 2019)) are no longer discernible from the current morphometric data.

This poses an interesting question, which requires further exploration: how enduring are the identified morphometric fingerprints (Table 1) over time? Additional future time-lapse bathymetric surveys could provide insights into the persistence of these fingerprints. Coupled with measurements of turbidity

TABLE 1 Identified morphometric fingerprints of channel-modifying features.

	Thalweg gradient (S)	Levee/wall slope (α_R, α_L)	Thalweg position (n_T)
Damming landslide	Decline and followed by a peak	Decreasing levee/wall slope	-
Sweep and swing meander	-	Correlation with phase lag to curvature	Correlation with phase lag to curvature
Knickpoint	Peak (no decline)	No change in levee/wall slope	-
Avulsion	Specific sections with different bankfull channel depth (H_B), bankfull width (B), sinuosity (SI), width-to-curvature (B/R), dimensionless meander wavelength (L/B) and levee slope (α_R, α_L)		

current activities, this approach might offer future perspectives on comprehending flow activity and channel-modifying processes in other systems solely through bathymetric mapping.

5.2 Systematic search in lower-resolution single surveys

Until now, the identification of landslide-dams relied on a few repeated surveys for qualitative assessments (Biscara et al., 2013; Pope et al., 2022b; Talling et al., 2022), or examinations of landslide scars or deposits (Babonneau et al., 2002; Smith et al., 2005; Mountjoy et al., 2009; Pope et al., 2022b). These methods are time-consuming and subject to individual judgement and interpretation. The identification of the previously unidentified landslide-dam at 40 km suggests that it is possible to systematically identify landslide-dams using single bathymetric surveys alone.

Comparison of bathymetric data at different resolutions shows that the higher resolution of 15 m in 2019 provides more accurate cross-sectional characteristics, particularly for levee/wall slopes (Figure 4E; Figure 9G–L; Supplementary Table S1) and thalweg position (Figure 4F; Figure 9M–R; Supplementary Table S1). However, lower resolution data (100 m in 1994/98) still reveals discernible trends and changes in morphometric characteristics, although with lower absolute values (e.g., mean levee/wall slope in the 1994/98 data is ~16° and in the 2019 data ~24°). Longitudinal characteristics (e.g., sinuosity, curvature or wavelength) are less affected by data resolution when a centerline is used as a reference axis, providing advantages over thalweg-based analyses (Shumaker et al., 2018; Bührig et al., 2022). This approach not only measures thalweg movement but also serves as a more independent reference axis as thalweg determination is highly dependent on resolution.

This makes the approach suitable for systems with low-resolution bathymetric data (Bührig et al., 2022). While absolute values at the cross-sectional level are resolution-dependent (Hasenhündl et al., 2023), trends and changes in characteristics provide valuable insights. The revealed fingerprints (Table 1) facilitate a systematic and efficient search for channel-modifying features within bathymetry data, without relying on visual inspection.

5.3 Morphodynamic reaches

The examination of the bankfull active channel and identified channel-modifying features allowed for the categorization of the Congo Canyon-Channel into three distinct morphodynamic reaches, as shown in Figure 10. It is noteworthy how constant the bankfull width (B) of the active channel remains throughout the Congo submarine system's extent (Figure 3D), while other morphometric characteristics vary across distinct reaches (Figure 3) (Hasenhündl et al., 2023). The upper reach (0–290 km) of the system within the incised canyon is characterized by higher thalweg gradients (S) (Figure 3B) and a marginally reduced cross-sectional area (A). Presuming, bankfull discharge, this likely reflects the higher driving forces for turbidity currents due to the steeper thalweg gradient (Konsoer et al., 2013). Evidently, these turbidity currents appear as erosive flows (Babonneau et al., 2004; Talling et al., 2022) typified by a dense frontal cell (Azpiroz-Zabala et al., 2017; Simmons et al., 2020; Pope et al., 2022a). Consequently, these flows erode the thalweg and the outer levees at the bend apices (Figure 9L), resulting in oversteepened active channel walls inside the canyon (wall slopes) and contributing to the triggering landslides and slumps from the canyon margins (Figure 10D). Landslides may be more common than previously thought (Babonneau et al., 2004). They have a significant impact on the active channel morphology within the canyon by damming the active channel, creating meander cut-offs and terraces (Pope et al., 2022b).

The steep drop downstream of a landslide dam (i.e., the knickpoint) can migrate upstream when subsequent turbidity currents travel over it once the area behind the blockage has been infilled. The migrating drop cuts into the backfill, creating terraces and re-excavating the infill material, similar to other knickpoints (Pope et al., 2022b; Talling et al., 2022). These channel-damming landslides likely occur on timescales of decades within the Congo Canyon-Channel, as evident from two similar-sized, well-preserved landslides at 40 km and 95 km. The frequency of such events in other canyon systems will likely depend on sediment delivery, tectonic regime, and local substrate characteristics. These blockages can store substantial quantities of sediment and other material. For instance, the landslide-dam at 40 km retains ~170
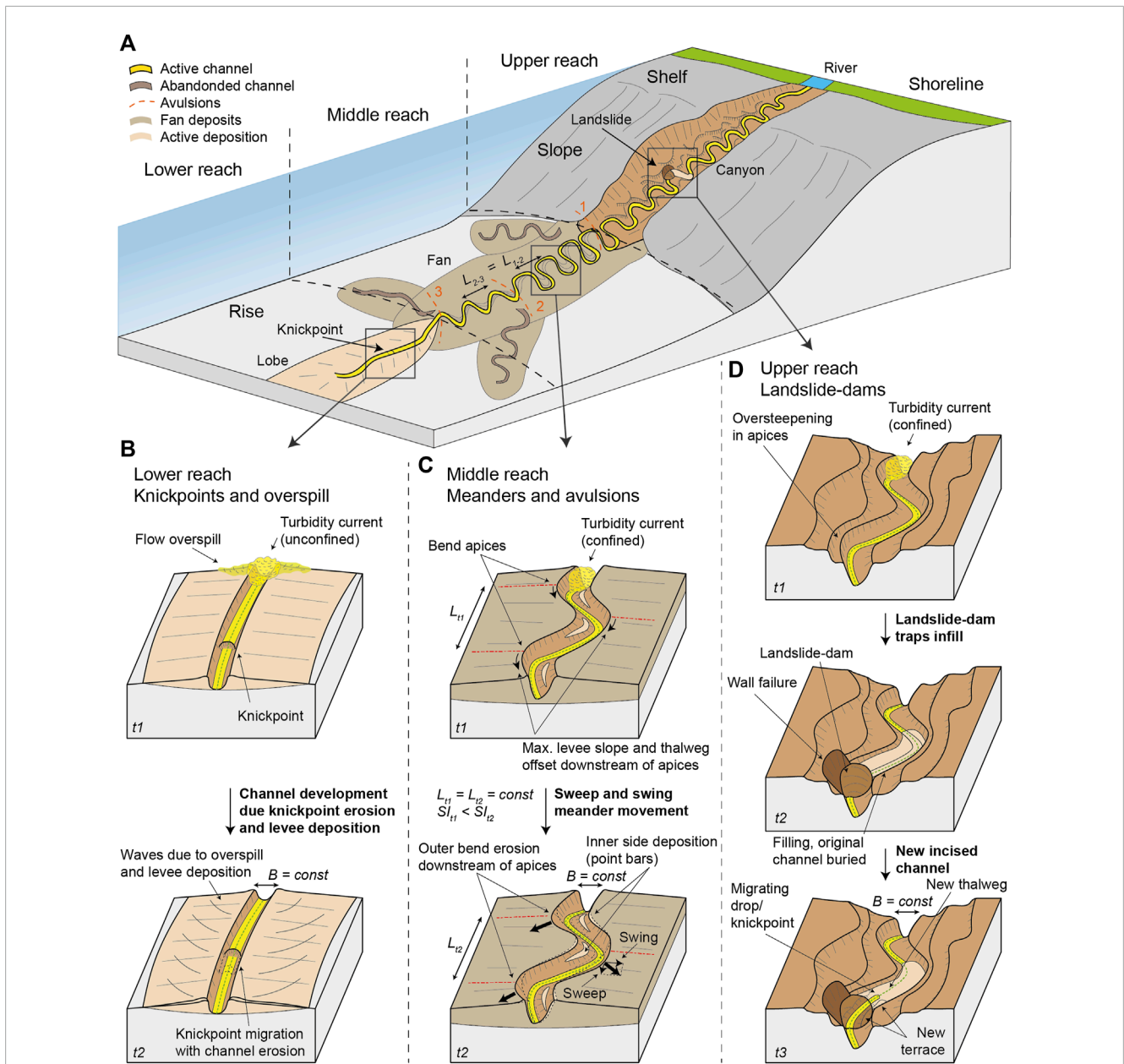
FIGURE 10
Division into three morphodynamic reaches based on identified channel-modifying features: **(A)** Overview of a submarine canyon-channel system like the Congo system. **(B)** Morphological evolution of the lower reach, the youngest and straightest part. The channel grows due to the constant overspill of unconfined turbidity currents. Upstream migrating knickpoints are probably the common channel-modifying features, causing stepwise material transport. **(C)** Morphological evolution of the middle reach with meanders and avulsions. The erosion of the outer bend downstream of the apices by the confined turbidity currents leads to sweep and swing meandering. This increases the sinuosity with channel age ($SI_{t1} < SI_{t2}$), but the wavelength remains the same over different ages ($L_{t1} = L_{t2}$ = const), separated by avulsions ($L_{1-2} = L_{2-3}$ = const). Material is continuously deposited on the inner sides (point bars) and eroded on the outer sides or bypassed. **(D)** Morphological evolution of the upper reach, the incised canyon. Oversteepening of the internal canyon walls in the apices possibly triggering channel-damming landslides. Material transported by turbidity currents is trapped by the infill and deposited permanently in newly formed terraces or stored temporarily and transported stepwise through upstream migrating steep drops, creating a new channel.

± 40 Mt of sediment (Pope et al., 2022b), equivalent to several years of sediment transported by the Congo River, which has an annual sediment flux of ~43 Mt (Milliman and Farnsworth, 2011; Pope et al., 2022b). Since these landslides leave fingerprints in the morphometric characteristics over decades, it is improbable that the current erosive flows can completely mobilize the accumulated material. Consequently, these landslides have a lasting impact on

the morphology, akin to the impacts observed in high alpine rivers and landslides (Korup, 2006). Even long runout flows observed in January and March 2020, did not excavate most of the infill upstream of the 95 km landslide-dam (Talling et al., 2022). Hence, a portion of the trapped material remains permanently deposited in newly formed terraces through the cutting of a new channel, while other parts are temporarily stored and stepwise transported through

upstream migrating steep drops, ultimately creating a new channel (Smith et al., 2005; Pope et al., 2022b).

Downstream of the upper canyon reach (290–900 km), morphometric characteristics remain uniform except for sinuosity (*SI*), which initially jumps to its highest values and then decreases down-system (Figure 4A). This is remarkable because different sections of varying ages, separated by avulsions (Picot et al., 2016), display similar thalweg gradient (*S*) (Figure 3B), channel depth (H_B) (Figure 3C), cross-sectional area (*A*) (Figure 3E), width-to-curvature ratio (*B/R*) (Figure 4B) and dimensionless meander wavelength (*L/B*) (Figure 4C). We interpret this uniformity as an equilibrium state for turbidity currents, completely contained within the channel. There are no obvious signs of excessive overspill (Figures 6D,F). This equilibrium state, free from the constraint of the canyon, facilitates the free formation of meanders. As sections of the channel become older, meanders become more pronounced (higher *SI* upstream, Figure 4A) (Kastens and Shor, 1986; Babonneau et al., 2010), resulting in sweep (downstream movement) and swing (outward movement) meanders, which are typical features observed in models (Peakall et al., 2000; Sylvester et al., 2011) and high curvature rivers (Sylvester et al., 2019) (Figure 10C). In contrast to the canyon upper reach, there is little evidence that sediment and material are trapped locally. Instead it is continuously deposited by the meandering movement on the inner margins (point bars) (Babonneau et al., 2010) and eroded from the outer margins or bypassed by the turbidity current throughout the entire reach. No evidence is apparent in the bathymetric data of side-wall collapses in the middle reach comparable with those observed in seismic cross-sections from other systems (Lewis et al., 1998).

In the youngest part of the channel, located further downstream (900–1,117.5 km), all characteristics change except for thalweg gradients (*S*) and bankfull width (*B*) (Figure 3). These changes support the views on the age and development of submarine channels (Konsoer et al., 2013; Shumaker et al., 2018; Jobe et al., 2020; Hasenhündl et al., 2023). Submarine channels begin relatively straight with a fixed channel width (Figure 3D) while their channel depth (H_B) gradually increases (Figure 3C) due to continuous turbidity current overspill, as indicated by the sediment waves. (Figures 7D,F; Figure 10B). Consequently, the slope of the levees develops due to levee aggradation (Figure 4E). Once a certain H_B and age are reached, turbidity currents are confined by the channel and lateral movements begin. This leads to the development of meanders, as observed upstream in sinuosity (*SI*) (Figure 4A) and width-to-curvature ratio (*B/R*) (Figure 4B).

In this straighter reach, probable upstream migrating knickpoints become the common channel-modifying features (Figure 10B), observed for the first time at this water depth (ca. 4,600 m). These knickpoints may form at the transition between channel and lobe (Heijnen et al., 2020) and exhibit upstream migration at a rate comparable to other submarine channels (a few kilometers per decade). This rate is much faster than the 0.001–1 m/year in rivers (Guiastrennec-Faugas et al., 2020; Heijnen et al., 2020). However, no knickpoints have been identified upstream in the middle reach (290–900 km), where swing and sweep of meander evolution dominates. This is in contrast to other systems, such as Bute Inlet or Knight Inlet (Gales et al., 2019; Heijnen et al., 2020), where knickpoints have been observed. In those systems, knickpoints appear to be able to migrate throughout the entire channel reach. It is therefore surprising that these features

fail to do similar in the Congo Canyon-Channel, although local disturbances have led to their generation in the upper reach (e.g., landslides, (Pope et al., 2022b)). In the lower reach, their upstream migration leads to stepwise material transport along the channel bed (Heijnen et al., 2022), accompanied by deposition due to levee overspill and on the lobe.

The morphodynamic reaches identified in this study are characterized by common channel-modifying features. The results show that sediment and material transport downslope within a canyon-channel system occurs at staggered intervals and can differ across various morphodynamic reaches. This enhanced understanding of the Congo submarine system's morphodynamics, which is likely applicable to similar systems, can help better position seabed infrastructure such as cables. Identifying specific morphodynamic reaches is critical to prevent damage to infrastructure, as processes such as channel-damming landslides or knickpoints can cause significant local erosion that could undermine cables (Talling et al., 2022).

6 Conclusion

In this study, we use the first repeat bathymetric surveys of one of the largest submarine canyon-channel systems (Congo submarine system, offshore West Africa), alongside an analysis of 12 morphometric characteristics of the bankfull active channel. Our analysis delineates distinctive morphometric fingerprints of channel-modifying features. Damming landslides can be identified by increased thalweg elevation, accompanied by a drop in thalweg gradient (*S*) and decreasing levee/wall slopes (α_R, α_L) upstream of the landslide, followed by a peak in *S*. Knickpoints can also be detected by a thalweg gradient peak; however, unlike landslides, they do not exhibit changes in levee/wall slope. A phase lag in thalweg position (n_T) and levee/wall slope (α_R, α_L) enables the identification of swing and sweep meanders. Furthermore, abrupt changes in several morphometric characteristics such as sinuosity (*SI*), bankfull channel depth (H_B), width-to-curvature ratio (*B/R*) and meander wavelength (*L/B*), indicate occurrences of avulsions, mainly for those that are less than ~6 kyr old in the Congo submarine system.

The morphometric fingerprints identified in this study offer a valuable framework for systematically detecting channel-modifying features in other existing bathymetric datasets. This overcomes the need for rare repeated bathymetric datasets or high-resolution surveys. In the Congo Canyon-Channel, our approach unveiled a previously unnoticed damming landslide (80 m thick and upstream reaching 20 km infill) within older 100 m resolution single survey data from 1994, underscoring the efficacy of this methodological approach.

By utilizing the morphometric characteristics and location of these channel-modifying features, we identified three distinct morphodynamic reaches in the Congo Canyon-Channel. In the canyon upper reach (0–290 km), channel damming landslides are common features, likely triggered by erosive flows. These landslides, which occur perhaps on timescales of decades, can temporarily store sediment and material equivalent to several years' of transported loads from the Congo River. Moving into the meandering middle reach (290–900 km), sweep and swing meanders are the predominant channel-modifying features. Their

development depends on their age, influenced by the occurrence of avulsions. Here, sediment and material undergo continuous deposition and erosion through meandering movement (outer bend erosion, point bar deposition) or they are bypassed by turbidity currents across the entire reach. In the developing lower reach (900–1,117.5 km), a few kilometers per decade upstream migrating knickpoint likely characterizes this straighter reach. This reach aligns with the progressive development of submarine channels, starting relatively straight with a fixed bankfull width (B) and growing in channel depth (H_B) due to constant turbidity current overspill. Material transport in this reach occurs primarily through stepwise upstream migration of knickpoints, accompanied by material deposition from overspill and lobe deposition.

These morphodynamic reaches illustrate that sediment and material transport downslope a canyon-channel system occurs in stages, and processes can vary spatially across different morphodynamic reaches. Furthermore, identifying reaches and their associated channel-modifying features can enhance understanding of morphodynamics and material transport in other submarine systems. This information can also provide valuable insights for establishing resilient seabed infrastructure.

Data availability statement

The multibeam data from JC187 (2019) are available to download via the British Oceanographic Data Centre (BODC) at https://doi.org/10.5285/dfe7a980-89d8-2830-e053-17d1a68b81ba. The multibeam data collected by Ifremer Geo-Ocean can be accessed via http://dx.doi.org/10.12770/d1076601-82a9-42a2-9d30-d0be8b2481a7. The modified Matlab script [original version by Hasenhündl and Blanckaert (2022), CC BY-SA 4.0] for this study can be found at https://gitlab.tuwien.ac.at/martin.hasenhuendl/matlab-script-for-the-morphometric-analysis.

Author contributions

MH: Conceptualization, Data curation, Formal Analysis, Investigation, Methodology, Software, Visualization, Writing–original draft, Writing–review and editing. PT: Conceptualization, Funding acquisition, Investigation, Project administration, Supervision, Writing–review and editing, Formal Analysis, Methodology, Writing–original draft. EP: Conceptualization, Data curation, Investigation, Methodology, Writing–review and editing, Formal Analysis, Supervision. MB: Conceptualization, Investigation, Project administration, Writing–review and editing, Formal Analysis. MSH: Investigation, Writing–review and editing, Formal Analysis. SR: Data curation, Investigation, Writing–review and editing, Formal Analysis. RdS: Conceptualization, Funding acquisition, Investigation, Project administration, Writing–review and editing, Supervision. AG: Data curation, Writing–review and editing. SH: Investigation, Writing–review and editing. SS: Investigation, Writing–review and editing. CH: Investigation, Writing–review and editing. CM: Investigation, Writing–review and editing. MAC: Writing–review and editing, Conceptualization, Funding acquisition. MC: Writing–review and editing Conceptualization, Funding acquisition.

Funding

Acknowledgments

Conflict of interest

Author CH was employed by Expert Analytics.

The remaining authors declare that the research was conducted in the absence of any commercial or financial relationships that could be construed as a potential conflict of interest.

Publisher's note

Supplementary material

The Supplementary Material for this article can be found online at: https://www.frontiersin.org/articles/10.3389/feart.2024.1381019/full#supplementary-material

References

Amir, A., Kenyon, N. H. N. H., Cramp, A., and Kidd, R. B. (1996). Morphology of channel-levee systems on the indus deep-sea fan, arabian sea. *Pak. J. Hydrocarb. Res.* 8, 43–53. Available at: https://pjhr.org.pk/index.php/pjhr/article/view/97/89

Azpiroz-Zabala, M., Cartigny, M. J. B. B., Talling, P. J., Parsons, D. R., Sumner, E. J., Clare, M. A., et al. (2017). Newly recognized turbidity current structure can explain prolonged flushing of submarine canyons. *Sci. Adv.* 3, e1700200. doi:10.1126/sciadv.1700200

Babonneau, N., Savoye, B., Cremer, M., and Bez, M. (2004). Multiple terraces within the deep incised Zaire Valley (ZaïAngo Project): are they confined levees? *Geol. Soc. Spec. Publ.* 222, 91–114. doi:10.1144/GSL.SP.2004.222.01.06

Babonneau, N., Savoye, B., Cremer, M., and Bez, M. (2010). Sedimentary architecture in meanders of a submarine channel: detailed study of the present Congo turbidite channel (zaiango project). *J. Sediment. Res.* 80, 852–866. doi:10.2110/jsr.2010.078

Babonneau, N., Savoye, B., Cremer, M., and Klein, B. (2002). Morphology and architecture of the present canyon and channel system of the Zaire deep-sea fan. *Mar. Pet. Geol.* 19, 445–467. doi:10.1016/S0264-8172(02)00009-0

Baudin, F., Martinez, P., Dennielou, B., Charlier, K., Marsset, T., Droz, L., et al. (2017). Organic carbon accumulation in modern sediments of the Angola basin influenced by the Congo deep-sea fan. *Deep. Res. Part II Top. Stud. Oceanogr.* 142, 64–74. doi:10.1016/j.dsr2.2017.01.009

Biscara, L., Mulder, T., Hanquiez, V., Marieu, V., Crespin, J.-P., Braccini, E., et al. (2013). Morphological evolution of Cap Lopez Canyon (Gabon): illustration of lateral migration processes of a submarine canyon. *Mar. Geol.* 340, 49–56. doi:10.1016/j.margeo.2013.04.014

Bührig, L. H., Colombera, L., Patacci, M., Mountney, N. P., and McCaffrey, W. D. (2022). Tectonic influence on the geomorphology of submarine canyons: implications for deep-water sedimentary systems. *Front. Earth Sci.* 10, 1–30. doi:10.3389/feart.2022.836823

Carter, L., Gavey, R., Talling, P., and Liu, J. (2014). Insights into submarine geohazards from breaks in subsea telecommunication cables. *Oceanography* 27, 58–67. doi:10.5670/oceanog.2014.40

Casalbore, D., Falcini, F., Martorelli, E., Morelli, E., Bosman, A., Calarco, M., et al. (2018). Characterization of overbanking features on the lower reach of the Gioia-Mesima canyon-channel system (southern Tyrrhenian Sea) through integration of morpho-stratigraphic data and physical modelling. *Prog. Oceanogr.* 169, 66–78. doi:10.1016/j.pocean.2018.02.020

Clare, M. A., Yeo, I. A., Bricheno, L., Aksenov, Y., Brown, J., Haigh, I. D., et al. (2023). Climate change hotspots and implications for the global subsea telecommunications network. *Earth-Science Rev.* 237, 104296. doi:10.1016/j.earscirev.2022.104296

Constantine, J. A., Dunne, T., Ahmed, J., Legleiter, C., and Lazarus, E. D. (2014). Sediment supply as a driver of river meandering and floodplain evolution in the Amazon Basin. *Nat. Geosci.* 7, 899–903. doi:10.1038/ngeo2282

Coynel, A., Seyler, P., Etcheber, H., Meybeck, M., and Orange, D. (2005). Spatial and seasonal dynamics of total suspended sediment and organic carbon species in the Congo River. *Glob. Biogeochem. Cycles* 19, GB4019. doi:10.1029/2004GB002335

Deptuck, M. E., Sylvester, Z., Pirmez, C., and O'Byrne, C. (2007). Migration–aggradation history and 3-D seismic geomorphology of submarine channels in the Pleistocene Benin-major Canyon, western Niger Delta slope. *Mar. Pet. Geol.* 24, 406–433. doi:10.1016/j.marpetgeo.2007.01.005

Gales, J. A., Talling, P. J., Cartigny, M. J. B., Hughes Clarke, J., Lintern, G., Stacey, C., et al. (2019). What controls submarine channel development and the morphology of deltas entering deep-water fjords? *Earth Surf. Process. Landforms* 44, 535–551. doi:10.1002/esp.4515

Galy, V., France-Lanord, C., Beyssac, O., Faure, P., Kudrass, H., and Palhol, F. (2007). Efficient organic carbon burial in the Bengal fan sustained by the Himalayan erosional system. *Nature* 450, 407–410. doi:10.1038/nature06273

Guiastrennec-Faugas, L., Gillet, H., Peakall, J., Dennielou, B., Gaillot, A., and Jacinto, R. S. (2021). Initiation and evolution of knickpoints and their role in cut-and-fill processes in active submarine channels. *Geology* 49, 314–319. doi:10.1130/G48369.1

Guiastrennec-Faugas, L., Gillet, H., Silva Jacinto, R., Dennielou, B., Hanquiez, V., Schmidt, S., et al. (2020). Upstream migrating knickpoints and related sedimentary processes in a submarine canyon from a rare 20-year morphobathymetric time-lapse (Capbreton submarine canyon, Bay of Biscay, France). *Mar. Geol.* 423, 106143. doi:10.1016/j.margeo.2020.106143

Hansen, L. A. S., Callow, R. H. T., Kane, I. A., Gamberi, F., Rovere, M., Cronin, B. T., et al. (2015). Genesis and character of thin-bedded turbidites associated with submarine channels. *Mar. Pet. Geol.* 67, 852–879. doi:10.1016/j.marpetgeo.2015.06.007

Harris, P. T., and Whiteway, T. (2011). Global distribution of large submarine canyons: geomorphic differences between active and passive continental margins. *Mar. Geol.* 285, 69–86. doi:10.1016/j.margeo.2011.05.008

Hasenhündl, M., Bauernberger, L. S., and Böhm, C. (2023). Extending morphometric scaling relationships: the role of bankfull width in unifying subaquatic channel morphologies. *Front. Earth Sci.* 11. doi:10.3389/feart.2023.1290509

Hasenhündl, M., and Blanckaert, K. (2022). A Matlab script for the morphometric analysis of subaerial, subaquatic and extra-terrestrial rivers, channels and canyons. *Comput. Geosci.* 162, 105080. doi:10.1016/j.cageo.2022.105080

Heijnen, M. S., Clare, M. A., Cartigny, M. J. B., Talling, P. J., Hage, S., Lintern, D. G., et al. (2020). Rapidly-migrating and internally-generated knickpoints can control submarine channel evolution. *Nat. Commun.* 11, 3129. doi:10.1038/s41467-020-16861-x

Heijnen, M. S., Clare, M. A., Cartigny, M. J. B., Talling, P. J., Hage, S., Pope, E. L., et al. (2022). Fill, flush or shuffle: how is sediment carried through submarine channels to build lobes? *Earth Planet. Sci. Lett.* 584, 117481. doi:10.1016/j.epsl.2022.117481

Heiniö, P., and Davies, R. J. (2007). Knickpoint migration in submarine channels in response to fold growth, western Niger Delta. *Mar. Pet. Geol.* 24, 434–449. doi:10.1016/j.marpetgeo.2006.09.002

Ifremer Geo-Ocean (2018). *Bathymetry - Congo fan (synthesis, 2013).* doi:10.12770/d1076601-82a9-42a2-9d30-d0be8b2481a7

Jobe, Z. R., Howes, N. C., Straub, K. M., Cai, D., Deng, H., Laugier, F. J., et al. (2020). Comparing aggradation, superelevation, and avulsion frequency of submarine and fluvial channels. *Front. Earth Sci.* 8. doi:10.3389/feart.2020.00053

Kane, I. A., and Clare, M. A. (2019). Dispersion, accumulation, and the ultimate fate of microplastics in deep-marine environments: a review and future directions. *Front. Earth Sci.* 7. doi:10.3389/feart.2019.00080

Kastens, K. A., and Shor, A. N. (1986). Evolution of a channel meander on the Mississippi deep-sea fan. *Mar. Geol.* 71, 165–175. doi:10.1016/0025-3227(86)90037-X

Khripounoff, A., Vangriesheim, A., Babonneau, N., Crassous, P., Dennielou, B., and Savoye, B. (2003). Direct observation of intense turbidity current activity in the Zaire submarine valley at 4000 m water depth. *Mar. Geol.* 194, 151–158. doi:10.1016/S0025-3227(02)00677-1

Kolla, V. (2007). A review of sinuous channel avulsion patterns in some major deep-sea fans and factors controlling them. *Mar. Pet. Geol.* 24, 450–469. doi:10.1016/j.marpetgeo.2007.01.004

Konsoer, K., Zinger, J., and Parker, G. (2013). Bankfull hydraulic geometry of submarine channels created by turbidity currents: relations between bankfull channel characteristics and formative flow discharge. *J. Geophys. Res. Earth Surf.* 118, 216–228. doi:10.1029/2012JF002422

Korup, O. (2006). Rock-slope failure and the river long profile. *Geology* 34, 45. doi:10.1130/G21959.1

Lemay, M., Grimaud, J.-L., Cojan, I., Rivoirard, J., and Ors, F. (2020). Geomorphic variability of submarine channelized systems along continental margins: comparison with fluvial meandering channels. *Mar. Pet. Geol.* 115, 104295. doi:10.1016/j.marpetgeo.2020.104295

Leopold, L. B., and Wolman, M. G. (1960). River meanders. *Bull. Geol. Soc. Am.* 71, 769–793. doi:10.1130/0016-7606(1960)71[769:RM]2.0.CO;2

Lewis, K. B., Collot, J., and Lallem, S. E. (1998). The dammed Hikurangi Trough: a channel-fed trench blocked by subducting seamounts and their wake avalanches (New Zealand–France GeodyNZ Project). *Basin Res.* 10, 441–468. doi:10.1046/j.1365-2117.1998.00080.x

Milliman, J. D., and Farnsworth, K. L. (2011). *River discharge to the coastal ocean: a global synthesis*. Cambridge University Press. doi:10.1017/CBO9780511781247

Morelli, E., Martorelli, E., Casalbore, D., and Chiocci, F. L. (2022). Morpho-stratigraphic evolution of a tectonically controlled canyon-channel system in the gioia basin (southern tyrrhenian sea). *Mar. Geol.* 451, 106881. doi:10.1016/j.margeo.2022.106881

Mountjoy, J. J., Barnes, P. M., and Pettinga, J. R. (2009). Morphostructure and evolution of submarine canyons across an active margin: Cook Strait sector of the Hikurangi Margin, New Zealand. *Mar. Geol.* 260, 45–68. doi:10.1016/j.margeo.2009.01.006

Ortiz-Karpf, A., Hodgson, D. M., and McCaffrey, W. D. (2015). The role of mass-transport complexes in controlling channel avulsion and the subsequent sediment dispersal patterns on an active margin: the Magdalena Fan, offshore Colombia. *Mar. Pet. Geol.* 64, 58–75. doi:10.1016/j.marpetgeo.2015.01.005

Palm, F. A., Peakall, J., Hodgson, D. M., Marsset, T., Silva Jacinto, R., Dennielou, B., et al. (2021). Width variation around submarine channel bends: implications for sedimentation and channel evolution. *Mar. Geol.* 437, 106504. doi:10.1016/j.margeo.2021.106504

Peakall, J., McCaffrey, B., and Kneller, B. (2000). A process model for the evolution, morphology, and architecture of sinuous submarine channels: PERSPECTIVES. *SEPM J. Sediment. Res.* 70. doi:10.1306/D4268C20-2B26-11D7-8648000102C1865D

Peakall, J., and Sumner, E. J. (2015). Submarine channel flow processes and deposits: a process-product perspective. *Geomorphology* 244, 95–120. doi:10.1016/j.geomorph.2015.03.005

Picot, M., Droz, L., Marsset, T., Dennielou, B., and Bez, M. (2016). Controls on turbidite sedimentation: insights from a quantitative approach of submarine channel and lobe architecture (Late Quaternary Congo Fan). *Mar. Pet. Geol.* 72, 423–446. doi:10.1016/j.marpetgeo.2016.02.004

Picot, M., Marsset, T., Droz, L., Dennielou, B., Baudin, F., Hermoso, M., et al. (2019). Monsoon control on channel avulsions in the late quaternary Congo fan. *Quat. Sci. Rev.* 204, 149–171. doi:10.1016/j.quascirev.2018.11.033

Pierdomenico, M., Bernhardt, A., Eggenhuisen, J. T., Clare, M. A., Lo Iacono, C., Casalbore, D., et al. (2023). Transport and accumulation of litter in submarine canyons: a geoscience perspective. *Front. Mar. Sci.* 10, 1–22. doi:10.3389/fmars.2023.1224859

Pirmez, C., Beaubouef, R. T., Friedmann, S. J., and Mohrig, D. C. (2000). "Equilibrium profile and baselevel in submarine channels: examples from late pleistocene systems and implications for the architecture of deepwater reservoirs," in *Deep-water reservoirs of the world: 20th annual* (Claremore, OK, USA: Society Of Economic Paleontologists And Mineralogists), 782–805. doi:10.5724/gcs.00.15.0782

Pirmez, C., and Flood, R. D. (1995). Morphology and structure of amazon channel. *Proc. Ocean. Drill. Program* 155. Initial Reports 155. doi:10.2973/odp.proc.ir.155.103.1995

Pope, E. L., Cartigny, M. J. B., Clare, M. A., Talling, P. J., Lintern, D. G., Vellinga, A., et al. (2022a). First source-to-sink monitoring shows dense head controls sediment flux and runout in turbidity currents. *Sci. Adv.* 8, eabj3220. doi:10.1126/sciadv.abj3220

Pope, E. L., Heijnen, M. S., Talling, P. J., Jacinto, R. S., Gaillot, A., Baker, M. L., et al. (2022b). Carbon and sediment fluxes inhibited in the submarine Congo Canyon by landslide-damming. *Nat. Geosci.* 15, 845–853. doi:10.1038/s41561-022-01017-x

Prerna, R., and Mahender, K. (2020). Geomorphometric comparison of submarine channel-levee complexes with fluvial river systems: observations from the Indus. *Geo-Marine Lett.* 40, 573–592. doi:10.1007/s00367-020-00654-8

Qin, Y., Alves, T. M., Constantine, J., and Gamboa, D. (2016). Quantitative seismic geomorphology of a submarine channel system in SE Brazil (Espírito Santo Basin): scale comparison with other submarine channel systems. *Mar. Pet. Geol.* 78, 455–473. doi:10.1016/j.marpetgeo.2016.09.024

Ruffell, S., Baker, M., Pope, E., and Talling, P. (2022). *Swath multibeam bathymetry surveys for Congo Submarine Canyon and Channel collected in 2019 and 2020, and changes in seabed elevation.* doi:10.5285/dfe7a980-89d8-2830-e053-17d1a68b81ba

Shumaker, L. E., Jobe, Z. R., Johnstone, S. A., Pettinga, L. A., Cai, D., and Moody, J. D. (2018). Controls on submarine channel-modifying processes identified through morphometric scaling relationships. *Geosphere* 14, 2171–2187. doi:10.1130/GES01674.1

Simmons, S. M. M., Azpiroz-Zabala, M., Cartigny, M. J. B. J. B., Clare, M. A. A., Cooper, C., Parsons, D. R. R., et al. (2020). Novel acoustic method provides first detailed measurements of sediment concentration structure within submarine turbidity currents. *J. Geophys. Res. Ocean.* 125, 1–24. doi:10.1029/2019JC015904

Smith, D. P., Ruiz, G., Kvitek, R., and Iampietro, P. J. (2005). Semiannual patterns of erosion and deposition in upper Monterey Canyon from serial multibeam bathymetry. *Geol. Soc. Am. Bull.* 117, 1123. doi:10.1130/B25510.1

Straub, K. M., Mohrig, D., McElroy, B., Buttles, J., and Pirmez, C. (2008). Interactions between turbidity currents and topography in aggrading sinuous submarine channels: a laboratory study. *Bull. Geol. Soc. Am.* 120, 368–385. doi:10.1130/B25983.1

Sylvester, Z., Durkin, P., Covault, J. A., and Sharman, G. R. (2019). High curvatures drive river meandering: REPLY. *Geology* 47, e486. doi:10.1130/G46838Y.1

Sylvester, Z., Pirmez, C., and Cantelli, A. (2011). A model of submarine channel-levee evolution based on channel trajectories: implications for stratigraphic architecture. *Mar. Pet. Geol.* 28, 716–727. doi:10.1016/j.marpetgeo.2010.05.012

Talling, P. J., Baker, M. L., Pope, E. L., Ruffell, S. C., Jacinto, R. S., Heijnen, M. S., et al. (2022). Longest sediment flows yet measured show how major rivers connect efficiently to deep sea. *Nat. Commun.* 13, 4193. doi:10.1038/s41467-022-31689-3

Talling, P. J., Cartigny, M. J. B., Pope, E., Baker, M., Clare, M. A., Heijnen, M., et al. (2023). Detailed monitoring reveals the nature of submarine turbidity currents. *Nat. Rev. Earth Environ.* 4, 642–658. doi:10.1038/s43017-023-00458-1

Tek, D. E., McArthur, A. D., Poyatos-Moré, M., Colombera, L., Patacci, M., Craven, B., et al. (2021). Relating seafloor geomorphology to subsurface architecture: how mass-transport deposits and knickpoint-zones build the stratigraphy of the deep-water Hikurangi Channel. *Sedimentology* 68, 3141–3190. doi:10.1111/sed.12890